Current Drive by Neutral Beams, Rotating Magnetic Fields and Helicity Injection in Compact Toroids

R. Farengo 1), A. F. Lifschitz 2), N. R. Arista 1) and R. A. Clemente 3)

1) Centro Atómico Bariloche e Instituto Balseiro, Bariloche, RN, Argentina
2) Consejo Nacional de Investigaciones Científicas y Técnicas, Argentina
3) Universidade Estadual de Campinas, Campinas, SP, Brasil

e-mail contact of main author: farengo@cab.cnea.gov.ar

Abstract. The use of neutral beams (NB) for current drive and heating in spheromaks, the relaxed states of flux core spheromaks (FCS) sustained by helicity injection and the effect of ion dynamics on rotating magnetic field (RMF) current drive in spherical tokamaks (ST) are studied.

1. Current Drive and Heating by Neutral Beam Injection in Spheromaks

Spheromaks are usually formed and sustained by helicity injection and the use of alternative methods is generally not considered. However, using NBs to drive part of the current could reduce the amplitude of the fluctuations needed to sustain the configuration, thus improving confinement, and provide additional control over the current profile. Finally, NBs will heat the plasma and provide a population of energetic particles that could improve the stability.

A Monte Carlo code was employed to study NB current drive and heating in spheromaks [1]. This code calculates the ionization of the neutral atoms and follows the exact trajectories of the ions (no gyro-averaging). Detailed studies of the ion orbits [2] have shown that the results obtained with the guiding center equations are qualitatively and quantitatively incorrect. Assuming a continuous injection of neutral particles, the code calculates their ionization, stopping and thermalization. This information is used to reconstruct the spatial distribution of beam density, current, transferred power and force in steady-state. The injection geometry is shown in Fig. 1. The beam is injected at the midplane and perpendicular to the geometrical axis. Setting the values of the neutral injection current (I_N), the energy of the neutral particles (E_N) and the impact parameter (b) the beam is completely determined.

The magnetic field and density profiles are determined by solving a Grad-Shafranov equation that contains the contribution of the beam. Assuming that the beam pressure is negligible compared to the plasma pressure the equilibrium equation can be written as:

$$r\frac{\partial}{\partial r}\left(\frac{1}{r}\frac{\partial \psi}{\partial r}\right)+\frac{\partial^2 \psi}{\partial z^2}=-16\pi^3 r^2\frac{dP}{d\psi}-\frac{8\pi^2}{c^2}\frac{dI_p^2}{d\psi}-\frac{8\pi^2}{c^2}\frac{d\left\langle I_{pd}\right\rangle^2}{d\psi}-\frac{8\pi^2 r}{c}\left\langle j_d\right\rangle$$

where ψ is the poloidal flux function, P is the plasma pressure, j_d is the toroidal current density driven by the beam, I_p is the poloidal plasma current, I_{pd} is the poloidal current driven by the beam and the angular brackets denote average over flux surfaces. The plasma current and pressure are related to the poloidal flux by:

$$I_p^2(\psi)=I_0^2\psi^2 \qquad P(\psi)=G_0\left[(\psi/\psi_0)-D(\psi/\psi_0)^2/2\right]$$

where I_0 and G_0 are constants, ψ_0 is the flux at the magnetic axis and D is the hollowness parameter. The plasma is considered to be inside a flux conserver of radius R_s and height Z_s and ψ is taken to be zero at the boundary. The equilibrium and the beam current are

calculated iteratively, keeping constant the average plasma density and the poloidal plasma current, until the solutions converge.

The results presented here were obtained with D=-0.5, r_s=z_s=0.5 m, r_0=0.31 m, n≈10^{20} m^{-3}, T_e= T_i =0.5 keV and B_{ext}= 7 kG. The current driven by the beam is the beam current minus the electron canceling current [3], which is due to drag of plasma electrons by the beam. The maximum cancelation occurs at the magnetic axis, where there are no electrons trapped in banana-like orbits. Fig. 2 shows the current carried by the beam and the total driven current, (i. e. beam current minus electron canceling current), per unit of injected power. The curves for Z_{eff}=1 and Z_{eff} =1.86 are displayed. The current presents a broad maximum around 40 keV. The beam current is higher for Z_{eff} =1 than for Z_{eff} =1.86, but the total driven current is lower in the former case. The reduction of the plasma effective charge does not result in an improvement in the total current drive efficiency because the reduction of the stopping cross section is compensated by an increase in the electron canceling current.

The beam current profiles are broad for injection with $b<r_0$, concentrated around the magnetic axis for $b≈r_0$ and hollow for $b>r_0$. The electron canceling current is larger for $b≈r_0$, because the beam concentrates in the region with smallest fraction of trapped electrons. For low Z_{eff}, the canceling current is almost half the beam current. The safety factor profiles of the self-consistent equilibria show a clear sensitivity to the impact parameter (Fig. 3). When $b>r_0$, the current concentrates around the axis thus reducing q_0. When $b>r_0$, the hollow current profile increases q_0. Finally, when $b<r_0$ there is a small reduction in q. The power deposition distribution can be controlled even with the simple injection geometries employed here, where only b is allowed to change. For injection below the magnetic axis ($b<r_0$), the power is deposited in a broad region that becomes more concentrated around the axis as b approaches to r_0. For $b>r_0$ the profile is hollow and the power deposited at the plasma core is small.

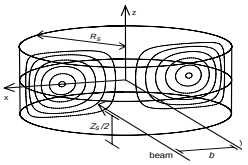

Fig. 1: Injection geometry

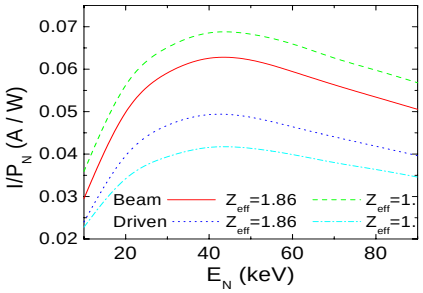

Fig. 2: Beam and driven current vs. En

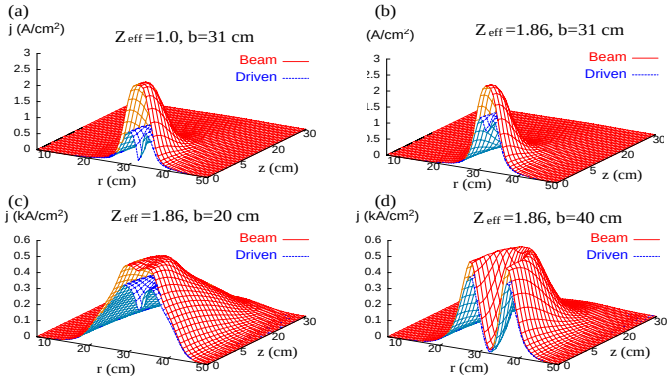

Fig. 4: Spatial distribution of beam and driven current density

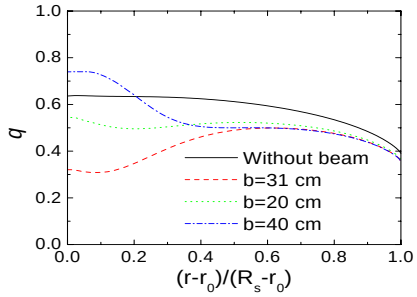

Fig. 3: Safety factor radial profile

2. Minimum Dissipation States in FCS Sustained by Helicity Injection

Relaxed states of a FCS sustained by d. c. helicity injection through magnetized electrodes were calculated by minimizing the Ohmic dissipation rate with the constraint of helicity

balance (injection rate=dissipation rate). The configuration considered, shown in Fig. 5, is a simplified version of the one proposed for the PROTO-SPHERA experiment [4]. It consists of a flux conserver which is grounded and covered on the inside with a dielectric and two electrodes which are insulated from the flux conserver and kept at voltages of $\pm V_{inj}/2$ by a power supply. The top and bottom of the flux conserver are rings of inner radius *b* and outer radius *a* and the side is a cylindrical shell of radius *a* and height *L*. The electrodes are circular, with radius *b*, and the entire configuration is axisymmetric ($\partial/\partial\theta\equiv 0$). We assume that a set of external coils, not shown in the figure, produce a uniform axial magnetic field ($B_{ext}\,\hat{z}$) on both electrodes. The external field at the electrodes, the voltage and the current flowing through the electrodes are considered external parameters that can be varied independently. To determine the minimum dissipation states with helicity balance as a constraint we introduce the following functional:

$$W_{dis} = \int \eta\, j^2 dV - \frac{\lambda}{\mu_0}\left[\int \eta\, \mathbf{j}\cdot\mathbf{B} dV + \int_{electrodes} \varphi\, \mathbf{B}\cdot\mathbf{dS}\right]$$

where η is the resistivity, λ is the Lagrange multiplier, $\varphi=\pm V_{inj}/2$ and SI units are employed. The second term on the RHS is the helicity dissipation rate and the third one, the helicity injection rate. The first variation of W_{dis} (δW_{dis}) can be written as the sum of a volume and a surface integral. The cancelation of the volume integral gives the Euler-Lagrane equation:

$$\nabla\times\left[\eta\left(2\mathbf{j}-\frac{\lambda}{\mu_0}\mathbf{B}\right)\right]-\lambda\eta\,\mathbf{j}=0$$

Using this equation, and $\nabla^2\mathbf{A}=-\mu_0\,\mathbf{j}$ a set of three coupled equations for j_θ, B_θ and A_θ is obtained. The boundary conditions needed to solve these equations are obtained from the cancellation of the surface term in δW_{dis} [5] and the physical situation considered. This gives: $\mathbf{B}.\hat{\mathbf{n}}=0$ and $\mathbf{j}.\hat{\mathbf{n}}=0$ at the flux conserver, B_θ(wall) determined by the current flowing through the electrodes and j_θ(wall)$=(\lambda/2\mu_0)\,B_\theta$(wall).

Two types of relaxed states, both with large regions of closed flux surfaces, were found: one has a central core formed by the flux that links the electrodes surrounded by a toroidal region of closed flux surfaces and the other has the open flux wrapped around the closed flux surfaces. Flux contours for both types of solutions are shown in Fig. 6 for V=600 ($V=V_{inj}\,\mu_0/|B_{ext}|\eta_0$), I=0.72 ($I=\mu_0 I_{ext}/a\pi|B_{ext}|$) and uniform resistivity ($\eta=10^{-6}$ Ωm). In Fig. 6a, λa=3.9228 while in Fig. 6b, λa=4.2948. The solutions shown in Figs. 6a and 6b have, respectively, $\lambda<\lambda_{eigen}$ and $\lambda>\lambda_{eigen}$, where $\lambda_{eigen}a$=4.0679 and corresponds to the solution with $\mathbf{j}.\hat{\mathbf{n}}=0$ everywhere at the boundary. These solutions are relative minima of the dissipation rate and the maximum corresponds to the limit when the injection and dissipation rates go to infinity and $\lambda\rightarrow\lambda_{eigen}$. The results presented below have V=600 and I=0.72 and correspond to the case with the open flux on the inside, which is the interesting one for the experiments.

Since the FCS contains regions of open and closed flux surfaces a resistivity profile that depends on the poloidal flux was employed: $\eta=\eta_0\left[1+|\psi|/|\psi_s|\right]^\alpha$ in the open flux region and $\eta=\eta_0\left[2-1.5\left(|\psi|-|\psi_s|/|\psi_0|\right)\right]^\alpha$ in the closed flux region, where ψ_s and ψ_0, are, respectively, the poloidal flux at the separatrix and at the magnetic axis. The parameter α controls the resistivity gradient (α=0 gives uniform resistivity). Fig. 7 shows resistivity profiles at the

midplane (z=0) obtained for α =0, 0.5, 1 and 2. As expected, when $\alpha \neq 0$, the resistivity is maximum at the separatrix and minimum at the magnetic axis. Fig. 8 shows radial profiles of j ($j=j_\theta \mu_0 a/|B_{ext}|$) for the same conditions as in Fig. 7. As α increases, the toroidal current density becomes more peaked and the maximum absolute value shifts outwards. Finally, Fig. 9. presents plots of the safety factor profile for the same conditions as in Fig. 7. For these calculations the safety factor profile is defined as: $q = (1/2\pi)\int (B/rB_p)ds$, where B_p is the normalized poloidal field and the integral is calculated following the field line around a single poloidal circuit. When α=0, uniform resistivity, q is maximum at the magnetic axis and decreases towards the edge. As α increases, the value at the magnetic axis decreases rapidly while the edge value shows a slight reduction for α=0.5 and 1 followed by an increase for α=2. This changes in the q-profile are clearly related to the changes in the current profile and total current already discussed. For α=2, a 50% increase in the external current (to I=1.08) increases the value of q at the magnetic axis by 18% and the value at the edge by 22%.

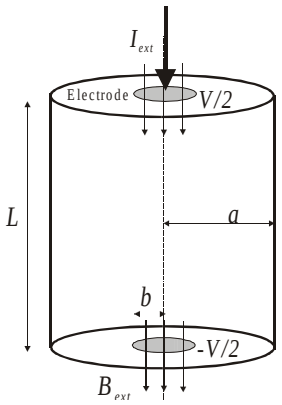

Fig. 5. Schematic diagram of the configuration considered

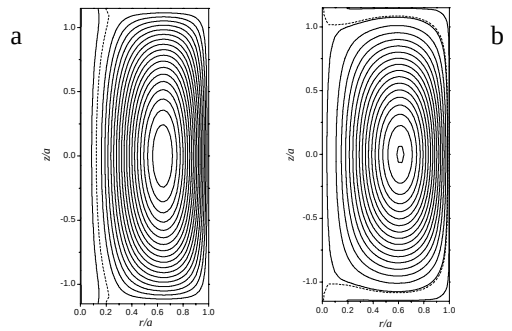

Fig. 6. Flux contours for both types of configurations

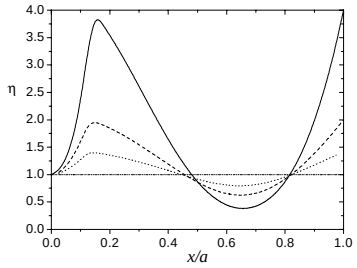

Fig. 7. Radial profiles of the resistivity at z=0

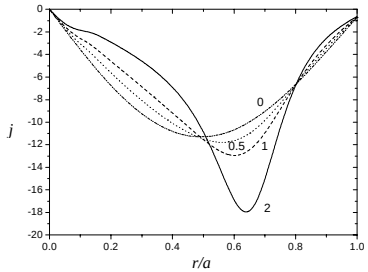

Fig. 8. Radial profiles of the toroidal current density at z=0

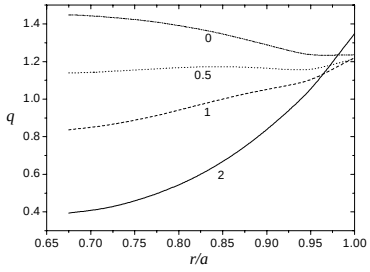

Fig. 9. Radial profiles of the safety factor at z=0

3. Rotating Magnetic Field Current Drive in Spherical Tokamaks

Rotating magnetic fields (RMF) have been used to form and sustain spherical tokamaks (ST) [6]. Previous theoretical studies on the use of this technique in configurations with an externally produced toroidal field have employed a model which assumes fixed ions and uniform density [7]. Here, we present initial results obtained with an MHD model with constant, uniform, temperature. The basic equations are similar to those employed in the study of RMF current drive in Field Reversed Configurations (FRC) [8]. The configuration considered is an infinitely long ($\partial/\partial z \equiv 0$), hollow, plasma column with inner radius b and outer radius a. A uniform axial current at the center of the column ($r<b$) produces a constant

toroidal field and a set of coils, localized very far from the plasma, a transverse rotating magnetic field. The results presented below were obtained using n=5x10^{18} m^{-3}, B_ω=20 G (RMF), B_v=60 G (vertical field), ω=0.5 MHz, η=10 $\eta_{Spitzer}$, a=0.22 m and T=30 eV. Except for the uncertainty in the resistivity, these parameters are indicative of those employed in the experiments [6]. Fig. 10 shows the efficiency (ratio between the total azimuthal current and the current that would be obtained if all the electrons rotate with uniform angular velocity) as a function of time for two values of B_{tor} (external toroidal field normalized to rotating field). In all cases, the dotted curves present the results obtained with the old model (fixed ions, uniform density) and the full lines the results obtained with the new model. As expected, the efficiency decreases when the toroidal field increases. The somewhat surprising result is that the inclusion of ion dynamics and non uniform density (new model) results in a higher efficiency. At this time, this is not fully understood. Fig. 11 shows radial plots of the toroidal current density ($\hat{j} = \mu\ a\ j_{tor} / B_\omega$) for the same conditions as in Fig. 10. We note that most of the current is localized near the outer plasma boundary but with the new model a second peak appears close to the inner boundary. This feature is also seen in the experiments (Fig. 6 in [6]).

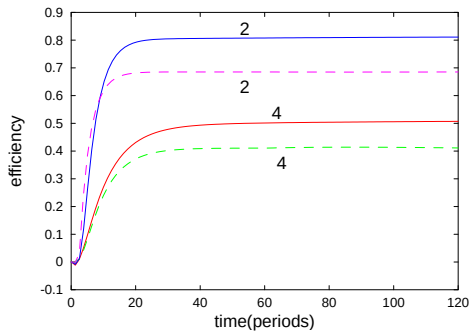

Fig. 10. Efficiency vs. time for B_{tor}=2 and 4.

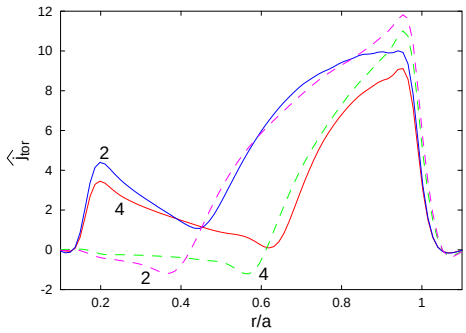

Fig. 11. Toroidal current density for B_{tor}=2 and 4.

Acknowledgements

This work was partially supported by the Agencia Nacional de Promoción Científica y Tecnológica of Argentina (PICT99-6509) and by IAEA contract N^o 10527/R3.

References

[1] "Monte Carlo simulation of neutral beam injection into a field reversed configuration" A. Lischitz, R. Farengo y N. Arista, *Nuclear Fusion* **42**, 863 (2002).

[2] “Numerical calculations of neutral beam injection in Spheromaks”. A. F. Lifschitz, R. Farengo y N. R. Arista, *Plasma Phys. and Contr. Fusion* **44**, 1979 (2002).

[3] “Numerical analisis of 2D MHD equilibrium with non-inductive plasma current in tokamaks”. K. Tani, M. Azumi and R. S. Devoto, *Journal of Computational Physics* **98**, 332 (1992).

[4] F. Alladio, Private communication 2000. The complete PROTO-SPHERA proposal can be downloaded from: http://www.frascati.enea.it/ProtoSphera.

[5] “Relaxed, minimum dissipation, states of a flux core spheromak sustained by helicity injection” R. Farengo and K. I. Caputi, *Plasma Phys. and Contr. Fusion* **44**, 1707 (2002).

[6] “Operation of the Rotamak as a Spherical Tokamak: The Flinders Rotamak-ST”. I.R. Jones, Chuanbao Deng, I.M. El-Fayoumi and P. Euripides, *Phys. Rev. Lett.* **81**, 2072 (1998)

[7] "Rotating magnetic field current drive in a hollow plasma column with a steady toroidal field". R. Farengo y R. Clemente, *Phys. Plasmas*, **8**, 1193 (2001).

[8] “A magnetohydrodynamic model of rotating magnetic field current drive in a field reversed configuration” R. D. Milroy, *Phys. Plasmas*, **7**, 4135 (2000).